5-21-2023

Evaluation of a Photodynamic Therapy Agent Using a Canine Prostate Cancer Model

Dong Luo
Case Western Reserve University, dxl576@case.edu

Xinning Wang
Case Western Reserve University, xxw171@case.edu

Gopalakrishnan Ramamurthy
Case Western Reserve University, gxr25@case.edu

Ethan Walker
Case Western Reserve University, yvv@case.edu

Lifang Zhang
Case Western Reserve University, lxz749@case.edu

See next page for additional authors

Recommended Citation

Luo D, Wang X, Ramamurthy G, et al.Evaluation of a photodynamic therapy agent using a canineprostate cancer model. The Prostate. 2023;83:1176-1185.doi:10.1002/pros.24560

Received: 9 February 2023 | Accepted: 4 May 2023

DOI: 10.1002/pros.24560

ORIGINAL ARTICLE

The Prostate WILEY

Evaluation of a photodynamic therapy agent using a canine prostate cancer model

Dong Luo PhD[1,2] | Xinning Wang PhD[3] | Gopalakrishnan Ramamurthy PhD[1] | Ethan Walker MD, PhD[3] | Lifang Zhang MD[1] | Aditi Shirke BSc[3] | Naraen G. Naidu[1] | Clemens Burda PhD[4] | Reena Shakya PhD[5] | Eric T. Hostnik DVM[6] | Mathew Joseph BSc[7] | Lee Ponsky MD[8] | Vladimir Ponomarev MD, PhD[9] | Thomas J. Rosol DVM, PhD[10] | Michael F. Tweedle PhD[11] | James P. Basilion PhD[1,3]

[1]Department of Radiology, Case Western Reserve University, Cleveland, Ohio, USA

[2]Department of Biomedical Science and Engineering, South China University of Technology, Guangzhou, China

[3]Department of Biomedical Engineering, Case Western Reserve University, Cleveland, Ohio, USA

[4]Department of Chemistry, Case Western Reserve University, Cleveland, Ohio, USA

[5]Target Validation Shared Resource, James Comprehensive Cancer Center, The Ohio State University, Columbus, Ohio, USA

[6]Department of Veterinary Clinical Sciences, College of Veterinary Medicine-Veterinary Medical Center, The Ohio State University, Columbus, Ohio, USA

[7]Interventional Cardiology Cath Core Lab, Davis Heart and Lung Research Institute, The Ohio State University, Columbus, Ohio, USA

[8]Department of Urology, University Hospitals, Cleveland Medical Center and Case Western Reserve University, Cleveland, Ohio, USA

[9]Department of Radiology, Memorial Sloan Kettering Cancer Center, New York City, New York, USA

[10]Department of Biomedical Sciences, Ohio University, Athens, Ohio, USA

[11]Department of Radiology, The Wright Center for Innovation in Biomolecular Imaging, The Ohio State University, Columbus, Ohio, USA

Correspondence
Dong Luo, PhD, Department of Biomedical Science and Engineering, South China University of Technology, Guangzhou International Campus, Guangzhou 511442, China.
Email: luodong09@scut.edu.cn

James P. Basilion, PhD, Department of Radiology, Case Western Reserve University, 11100 Euclid Ave, Cleveland, OH 44122, USA.
Email: jxb206@case.edu

Funding information
National Institutes of Health; National Foundation for Cancer Research

Abstract

Background: Male dogs can develop spontaneous prostate cancer, which is similar physiologically to human disease. Recently, Tweedle and coworkers have developed an orthotopic canine prostate model allowing implanted tumors and therapeutic agents to be tested in a more translational large animal model. We used the canine model to evaluate prostate-specific membrane antigen (PSMA)-targeted gold nanoparticles as a theranostic approach for fluorescence (FL) imaging and photodynamic therapy (PDT) of early stage prostate cancer.

Methods: Dogs (four in total) were immunosuppressed with a cyclosporine-based immunosuppressant regimen and their prostate glands were injected with Ace-1-hPSMA cells using transabdominal ultrasound (US) guidance. Intraprostatic tumors grew in 4–5 weeks and were monitored by ultrasound (US). When tumors reached an appropriate size, dogs were injected intravenously (iv) with PSMA-targeted nano

Dong Luo and Xinning Wang have contributed equally to this study.

agents (AuNPs-Pc158) and underwent surgery 24 h later to expose the prostate tumors for FL imaging and PDT. Ex vivo FL imaging and histopathological studies were performed to confirm PDT efficacy.

Results: All dogs had tumor growth in the prostate gland as revealed by US. Twenty-four hours after injection of PSMA-targeted nano agents (AuNPs-Pc158), the tumors were imaged using a Curadel FL imaging device. While normal prostate tissue had minimal fluorescent signal, the prostate tumors had significantly increased FL. PDT was activated by irradiating specific fluorescent tumor areas with laser light (672 nm). PDT bleached the FL signal, while fluorescent signals from the other unexposed tumor tissues were unaffected. Histological analysis of tumors and adjacent prostate revealed that PDT damaged the irradiated areas to a depth of 1–2 mms with the presence of necrosis, hemorrhage, secondary inflammation, and occasional focal thrombosis. The nonirradiated areas showed no visible damages by PDT.

Conclusion: We have successfully established a PSMA-expressing canine orthotopic prostate tumor model and used the model to evaluate the PSMA-targeted nano agents (AuNPs-Pc158) in the application of FL imaging and PDT. It was demonstrated that the nano agents allowed visualization of the cancer cells and enabled their destruction when they were irradiated with a specific wavelength of light.

KEYWORDS

canine prostate cancer, fluorescence imaging, nanoparticles, PDT, PSMA

1 | INTRODUCTION

Prostate cancer is the most diagnosed cancer among men, with an estimated 268,490 new cases and 34,500 new deaths in the United States for 2022.[1] With the use of prostate-specific antigen (PSA) testing, more prostate cancers can be detected at an early stage, expanding the time window for the patients to receive appropriate treatment. Whole gland radiotherapy and prostatectomy are the two mainstay treatment options.[2,3] The 5-year survival rate has greatly improved with early diagnosis and treatment. However, there still exists an urgent unmet clinical need to optimize the therapeutic options. Both radiotherapy and radical prostatectomy may cause severe side effects including chronic erectile dysfunction, incontinence, and diarrhea, due to the inevitable damage to the adjacent normal tissues.[4] One of the largest issues is local recurrence of cancer, likely resulting from undetected locally invasive prostate cancer that is not removed during the surgery (11%–48% incidence).[5] The recurrence of cancer may progress into metastatic castration-resistant prostate cancer (mCRPC), which has a very low cure rate with an average survival period of only approximately 3 years.[6,7]

There has been significant development in treatment strategies for prostate cancers. Over the past decade, diagnosis and therapy of prostate cancer have progressed rapidly to improve the treatment outcomes based on both the development of imaging technology and devices, as well as theranostic agents.[8–10] Imaging modalities, such as computed tomography (CT) and magnetic resonance imaging (MRI), can be combined with radiation sources to facilitate image-guided radiotherapy so malignant lesions can be more precisely localized for radiation dose delivery.[11–13] Moreover, radiosensitizers have been developed and employed for local radiation enhancement to reduce the overall dose and damage to surrounding normal tissues.[14,15] Fluorescence (FL) imaging probes have also been developed for fluorescent image-guided surgery, which helps the surgeon identify cancerous tissue, delineate tumor margins, and potentially significantly reduce the recurrence of prostate cancer.[16,17] Recently, near-infrared (NIR) probes, OTL78,[18] and IS-002 (https://clinicaltrials.gov/ct2/show/NCT04574401), which target prostate-specific membrane antigen (PSMA), have demonstrated excellent capability to highlight PSMA-positive tumors, and have entered clinical trials for FL-guided surgery.

Research on preclinical animal models of prostate cancer has enabled numerous breakthroughs, and a wide variety of transgenic, knockout, and xenograft mouse models have been developed.[19] The mouse models contribute greatly to the understanding of the biology of prostate cancer and provide a platform to evaluate the performance of various diagnostic and therapeutic agents before their clinical translation. However, prostate cancer is a complex and multifactorial disease process, and no ideal animal model is available to fully

recapitulate all the features of prostate cancer in men.[20] Compared to rodents, dogs are more genetically heterogeneous,[21] and are unique among laboratory animals in that intact male dogs develop benign prostatic hyperplasia (BPH) that progresses with age. Dogs are also the only animals that develop spontaneous prostate cancer that typically progresses to invasive and metastatic disease.[22] Bone metastases are common in late-stage disease and the cancers are usually androgen-insensitive.[23] The large relative size of the dog compared to rodents, and the anatomy and functional similarities of their prostate to that of men permit diagnostic and surgical procedures to be developed for both veterinary and human clinical practice.[24] Finally, prostate cancer in dogs can metastasize to bone and form osteoblastic metastases with new woven bone as seen in men.[25] Canine prostate cancer models are thus ideal to investigate relevant imaging and therapeutic agents.

PSMA is a unique biomarker and it is highly expressed in prostate cancer and its metastases.[26,27] We have previously used retrovirally transformed PSMA-expressing PC3 cancer models in rodents and used them to study optical, CT, and MRI of PSMA-targeted probes.[28–30] Significantly, our PSMA-targeted optical imaging probe using silicon phthalocyanine, a photosensitizer that has strong FL and can generate reactive oxygen species (ROS) for tumor ablation upon light irradiation, has demonstrated potential for FL image-guided surgery and adjuvant photodynamic therapy (PDT).[16] We can further control the release of this photosensitizer and its activities by conjugating it to PSMA-targeted gold nanoparticles via a cathepsin cleavable linker, which we have reported to have good tumor selectivity, free Pc158 release upon cathepsin cleavage and PDT efficacy in mouse models.[31,32] Therefore, we used a modified version of the recently developed orthotopic dog prostate cancer model[23] to investigate targeted FL imaging and PDT efficacy of PSMA-targeted nano agents, AuNPs-Pc158 (Supporting Information: Figure S1). These results demonstrated that PSMA-targeted gold nanoparticle delivery of PDT agents is both feasible and applicable in a large animal model resulting in the deposition of PDT agent in targeted tissue and destruction of tumor tissue when irradiated by NIR light.

2 | MATERIALS AND METHODS

2.1 | Nanoparticles synthesis

PSMA-targeted nano agents (AuNPs-Pc158) were synthesized and characterized as previously reported and used for dog orthotopic tumor FL imaging and PDT.[32] The Pc158 concentration was calculated according to its absorbance peak intensity to determine the injection dose for the four dogs (nos. 2, 3, 4, 5).

2.2 | Cell culture

Ace1 cells were derived from a spontaneous prostatic adenocarcinoma in a dog, and the derived cell line was shown to form osteoblastic bone metastases in nude mice after intracardiac injection and were provided by the Thomas Rosol laboratory (Ohio University).[33] Ace-1 cells express canine PSMA that are highly homologous to human proteins; however, the level of PSMA in Ace-1 cells is relatively low.[34] Transfection of human genes to Ace1 cells is readily achieved.[21] The Ace-1-hPSMA cells were created to enhance the expression of human PSMA in the Ace-1 cells by transformation using a retrovirus system and were kindly provided by Vladimir Ponomarev at Memorial Sloan Kettering Cancer Center. Ace-1-hPSMA cells were incubated at 37°C and 5% CO_2 in Roswell Park Memorial Institute 1640 medium supplemented with 10% fetal bovine serum (FBS) and 1% penicillin/streptomycin under a humidified atmosphere.[23]

2.3 | Binding of cell lines to *N*-[*N*-[(*S*)-1,3-dicarboxypropyl]carbamoyl]-*S*-[^{3}H]-methyl-L-cysteine (^{3}H-ZJ24)

The binding assay was performed as described previously[35] using ^{3}H-labeled *N*-[*N*-[(*S*)-1,3- dicarboxypropyl]carbamoyl]-L-cysteine (ZJ24), which is a well-known ligand/inhibitor against PSMA.[36] Briefly, cells (1×10^6) were incubated with different concentrations of ^{3}H-ZJ24 (GE Healthcare Life Sciences) in a total volume of 200 µL of 50 mM Tris buffer (pH 7.5) for 1 h at 37°C. The mixture was centrifuged at 3000*g* for 5 min at 4°C to separate bound and free ^{3}H-ZJ24. The supernatant was then removed, and the cell pellet was washed three times with 500 µL of cold Tris buffer and radioactivity of the pellet was then counted by scintillation counter. Nonspecific binding was determined using the same method in the presence of 0.1 mM ZJ24.

2.4 | Tumor model

Three- to six-year-old, uncastrated, healthy laboratory beagles were used for Ace-1-hPSMA cell implantation. Cell implantation into the prostate was completed as reported by Tweedle et al. and was guided by abdominal B mode ultrasound (US).[21] The Institutional Care and Use protocol number was 2013A00000081, approved at The Ohio State University. We implanted both lobes of the prostate to increase the tumor take rate. Each lobe received 1×10^7 Ace-1-hPSMA cells and tumors were usually observed in at least one lobe. Intraprostatic tumors grew in 4–5 weeks and were monitored by US. The tumor take rate was approximately 80% as only one dog in five failed to yield intraprostatic tumor after Ace-1-hPSMA injection into the gland and was not used in the study (dog no. 1 was omitted).

2.5 | FL imaging and PDT

When tumors grew locally for 4 weeks, PSMA-targeted nano agents (AuNPs-Pc158) were injected (IV) into the dogs and allowed to circulate for 24 h. The initial dose was calculated based on the

previous doses used for mice (0.1 mg/kg Pc158) and converted to a dog-relevant dose using surface area scale-up calculations.[37] After injection, the dogs were maintained for 24 h to allow the nano agents to accumulate in the tumors and release Pc158. The dogs were then anesthetized (using an approved protocol, OSU IACUC 2013A00000081) and underwent surgery to expose the prostate. The gland was imaged using a Curadel FL imaging device (Curadel LLC). Prostate tumors were identified by macroscopic observation by a veterinary pathologist, which always correlated with FL. The fluorescent areas and nonfluorescent normal tissues were masked with black paper to expose only a segment of the prostate tumor and a portion of normal tissues. The masked regions were then irradiated with light of 672 nm to generate the PDT effect in situ. The irradiation energy was 150 J/cm^2 based on mice studies (model 525 Laser Diode Driver, 1–5 mW/cm^2 of 672 nm light from a diode laser; Applied Optronics Corp.) equipped with a GRIN-lens-terminated multimode fiber (OZ Optics) (Supporting Information: Figure S2). After light irradiation, the tumor areas were imaged again using the Curadel FL imaging device (Supporting Information: Figure S2), and animals were monitored for 2 h to allow tissue damage induced by PDT to be detectable. The dog was then euthanized by an overdose of barbiturate and the prostate gland was removed, imaged ex vivo, and placed into 10% neutral-buffered formalin for histological processing.

2.6 | Histopathology

Following ex vivo imaging, the prostate gland and tumor tissues were fixed, embedded in paraffin, and stained with hematoxylin and eosin (H&E) for evaluation by histopathology. Tissue slides were examined by a veterinary pathologist to determine the effect of PDT on tumor tissues and were compared to nonirradiated tumor tissue. The effect of collateral damage to tissues surrounding the irradiated tumor, for example, vasculature and nerve tissue, were also examined to determine whether PDT of prostate tumor can be performed without destroying surrounding normal prostate tissues. The tissue slides were also silver-stained for the presence of AuNPs (Sigma Silver Enhancer Kit) followed by H&E standard procedures as reported previously,[32] and the FL signal from Pc158 was imaged directly using FL microscopy. On occasion, the FL signal was marked with pathology ink before fixation for later correlation with histology.

3 | RESULTS

3.1 | PSMA expression in Ace-1-hPSMA cells

The level of PSMA expression was first checked by western blot compared to Ace-1 cells, PC3pip cells, which are human prostate cancer PC3 cells retrovirally transfected with PSMA, and PC3flu cells, which are transfection control of PC3pip cells. PC3pip cells overexpress PSMA at levels found in nonmanipulated prostate cancer cells lines, for example, LNCaP cells and are widely used for mice studies.[4,28,29,31,32,38] PSMA expression was found in PC3pip and Ace-1-hPSMA cells. Level of PSMA expression in Ace-1-hPSMA cells was much lower than that in PC3pip cells. Ace-1 and PC3flu cells showed negligible amount of PSMA expression by western blot (Supporting Information: Figure S3). The number of PSMA receptors on the Ace-1-hPSMA cells was further determined using a ^{3}H-labeled PSMA ligand ZJ24.[35,36] Specific binding was only observed in PSMA-positive Ace-1-hPSMA and PC3pip cells, but not in Ace-1 and PC3flu cells (Table 1, Figure 1). The maximum binding capacity (Bmax) for Ace-1-hPSMA was 93,500 molecules/cell, and that for PC3pip cells was 216,800 molecules/cell. PSMA exists as a symmetric dimer that contains two identical binding sites for ^{3}H-ZJ24; therefore, the number of PSMA dimer receptor on each cells is estimated to be half of the Bmax.[39,40] Accordingly, each Ace-1-hPSMA cell had 46,750 PSMA receptors/cell and was much lower than that in PC3pip cells (108,400 PSMA receptors/cell). The results are consistent with western blot results.

3.2 | Tumor size and location verification

In humans, a suspicious PSA blood test is followed by a multiparametric MRI (MP-MRI), then a biopsy. A PSMA positron emission tomography (PET) scan is performed if the prior tests and Gleason score indicate a suspicion of aggressive disease that may have spread beyond the gland. In our study, no PSA test, MR scan, and PSMA PET scan were performed in the canine after Ace-1-hPSMA cell implantation. The growth of intraprostatic tumors was only monitored by US. It was found that the canine model consistently produced Ace-1-hPSMA tumors (0.5–3 cm) that originated in the interior of the prostate gland and often grew into and through the capsule of the prostate gland. In some dogs, a small (1–2 cm) subcutaneous tumor formed at the site

TABLE 1 PSMA expression on prostate cancer cells.

Cell line	Ace-1-hPSMA	Ace-1	PC3pip	PC3flu
Bmax (^{3}H-ZJ24 molecules/cell)	93,500 ± 600	ND	216,800 ± 4,400	ND
Number of PSMA receptor/cell	46,750 ± 300	ND	108,400 ± 2200	ND
Kd (nM)	33.9 ± 4.5	NA	43.5 ± 5.4	NA

Note: Data represent mean ± SD of triplicates.

Abbreviations: Bmax, maxium binding capacity; Kd, dissociation constant; NA, not available; ND, not detectable; PSMA, prostate-specific membrane antigen.

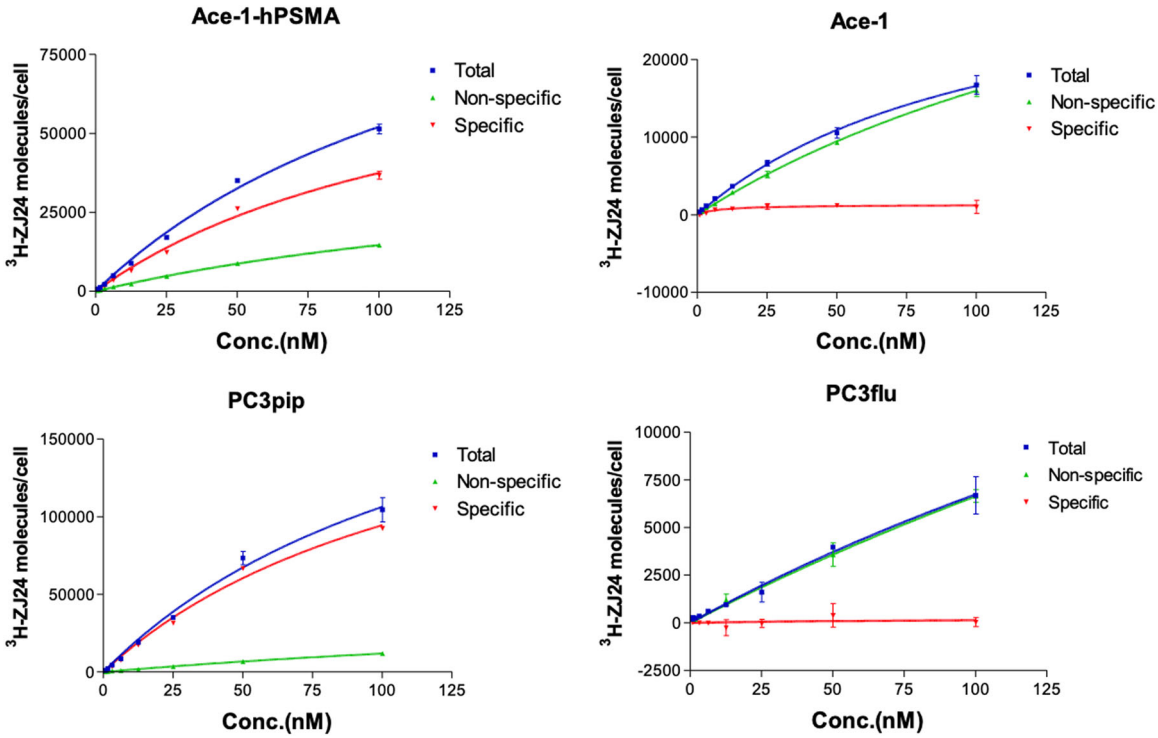

FIGURE 1 Binding of cells to ^{3}H-ZJ24. Cells (1×10^6) were incubated with various concentrations of ^{3}H-ZJ24 at 37°C. After 1 h of incubation, cells were washed with cold Tris buffer, and the radioactivity of the cell pellet was measured. Data represent mean ± SD of triplicates. [Color figure can be viewed at wileyonlinelibrary.com]

where the 22 G implantation needle passed through the subcutis, which was probably due to low-level tumor cell seeding. The prostate tumors were more firm than the soft surrounding prostate glandular tissue and could be identified by gross appearance and manual palpation. The firmness was likely due to reactive connective tissue stroma. The capsular tumors had greater amounts of stroma compared to intraprostatic tumors. Larger tumors often had central necrosis. Metastatic spread to regional lymphatics and local lymph nodes generally did not occur in the time frame of the experiments. Previous studies have demonstrated metastatic spread after the 4-week interval of tumor growth used in this study.[21]

3.3 | Fluorescent imaging of prostate tumor by AuNPs-Pc158

Fluorescent imaging is a sensitive method to detect cancer. By targeting PSMA, we have selectively identified PSMA-positive tumors by either a PSMA-targeted small molecule or nanoparticle-based FL imaging probes.[28,32] The dogs previously implanted with Ace-1-hPSMA cells received PSMA-targeted nano agents (AuNPs-Pc158) through IV injection 24 h before the surgery. The dogs underwent surgery to expose the prostate gland as shown in Figure 2A. Prostate tumors could often be seen as bulging lobulated mass from the capsule of the prostate glands. Using the Curadel FL imaging device, the intraprostatic, capsular, and extracapsular tumor tissue were fluorescent, while surrounding normal prostate tissues were not (Figure 2B and Supporting Information: Figure S4). Prostate tumors that were completely within the gland could also be identified by tumor FL through the capsule of the gland. In addition, subcutaneous tumors formed at the site where the needle passed through the subcutis were also highlighted by Pc158 FL (Supporting Information: Figure S5).

3.4 | PDT

Following FL imaging, but while the tumor and prostate remained in the dog, part of the tumor and a small area of normal prostate adjacent to the tumor were exposed to 150 J/cm^2 of 672 nm light for PDT treatment, while the remaining tumor and prostate were covered with opaque black paper (Figure 3A). After PDT, the prostate was imaged again. It was found that FL signal in the treated area was photobleached (Figure 3A), demonstrating the activation of Pc158 released from the PSMA-targeted AuNPs-Pc158. In contrast, the FL signal in the nonirradiated area had the same intensity as before therapy (Figure 3B). It was demonstrated that tissue damage from PDT was visible (1 h) after PDT and was detected histologically including using Caspase 3 staining,[41–44] therefore, after PDT, the dog was maintained under general anesthesia for 2 h before euthanasia. The prostate gland was then removed for ex vivo imaging. Ex vivo imaging results were consistent with the in vivo imaging results. FL signal was only observed in the untreated tumor, while the treated

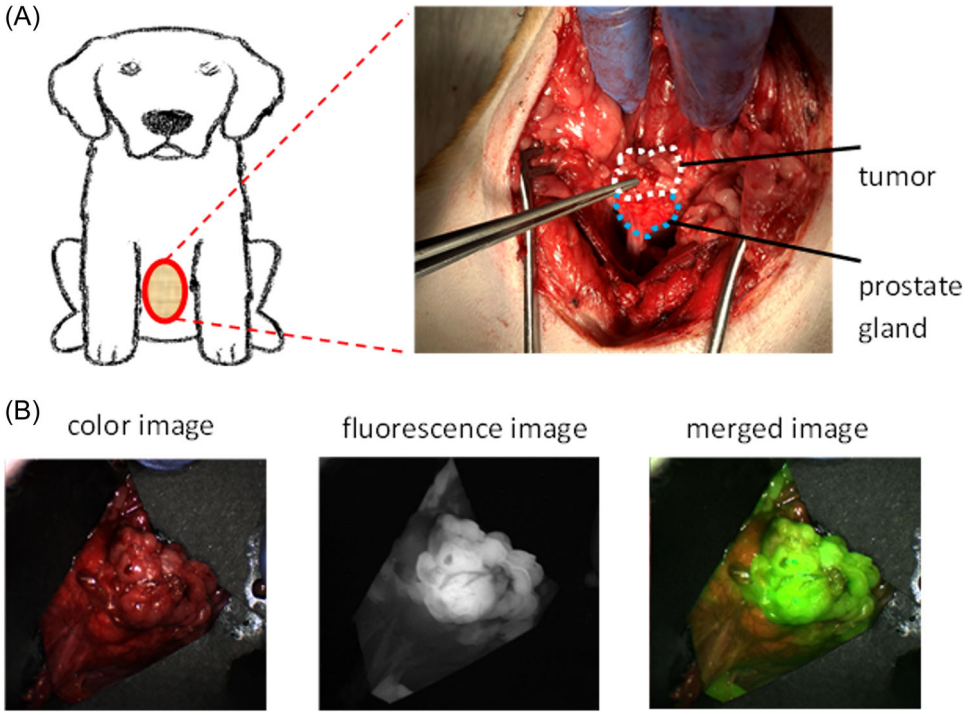

FIGURE 2 Representative FL images of prostate and Ace-1-hPSMA prostate tumor (Dog no.3). (A) Surgical site showing the ventral prostate and tumor. (B) Prostate gland and tumor in vivo under white light (left), in vivo FL image of the prostate gland and tumor (middle) and merged FL image with color image showing the highlight of tumor by nano agents (right). FL, fluorescence; PSMA, prostate-specific membrane antigen.

area and normal prostate did not have any FL (Figure 3B). These results indicated that the PSMA-targeted AuNPs-Pc158 could selectively accumulate and release Pc158 (as monitored by dequenching) in PSMA-expressing tumors, but not in normal prostate tissue. It also showed that PDT was a focal treatment since the FL in the treated area was bleached, while areas that were not irradiated remained fluorescent.

After ex vivo imaging of the whole prostate gland, it was then sequentially sectioned (5 mm slices) to expose cross-sections of the gland. As shown in Supporting Information: Figure S4, the tumor tissue protruded into and through the prostate capsule and could be clearly identified from the prostate parenchyma in the white light image. Under the FL imaging camera, FL signals originated from tumor tissue in the gland and capsule. The fluorescent areas were tumor tissue that had accumulated nano agents and free Pc158 released by cathepsin cleavage. As shown in Supporting Information: Figure S6, nano agents were stained and visible in the tumor tissues while absent in the normal prostate gland. The FL images and PDT treatment results for the other dogs (nos. 2, 4, 5) were also presented in Supporting Information: Figure S7–9.

3.5 | Histopathological analysis

Histopathological analysis of the tumor and the adjacent prostate showed that in the area of treatment, there was scattered tumor cell necrosis of the outer 1–2 mms of the tumors with multifocal hemorrhage and acute inflammation with neutrophils (Figure 4A). The histopathology revealed evidence of a treatment effect that included necrosis, hemorrhage, secondary inflammation, and occasionally focal thrombosis in the tumor capsule. In addition, independent of treatment, there was mononuclear inflammation around tumor cells that was consistent with a mild immune reaction from the dog. Bilateral tumor growth was consistently present in the dogs with tumor growth in the prostate lateral lobes and extension into the prostate capsule that extended beyond the normal margin of the prostate. There was no effect of PDT treatment on the adjacent normal prostate tissue that had the expected BPH (Figure 4B), which is typical in adult intact male dogs. It was concluded that only tumor tissue demonstrated enhanced FL and normal tissues, including BPH, had no increased FL.

4 | DISCUSSION

FL imaging of cancer biomarkers for early diagnosis of tumor lesions has the advantage of high sensitivity[45] and the use of photosensitizers has expanded its application to adjuvant therapy, such as FL-guided surgery and PDT.[46,47] In the development of most imaging or therapeutic agents, rodent animal models are used to evaluate their performance before clinical trials. Numerous rodent prostate tumor models have been developed and biomarkers such as PSMA have

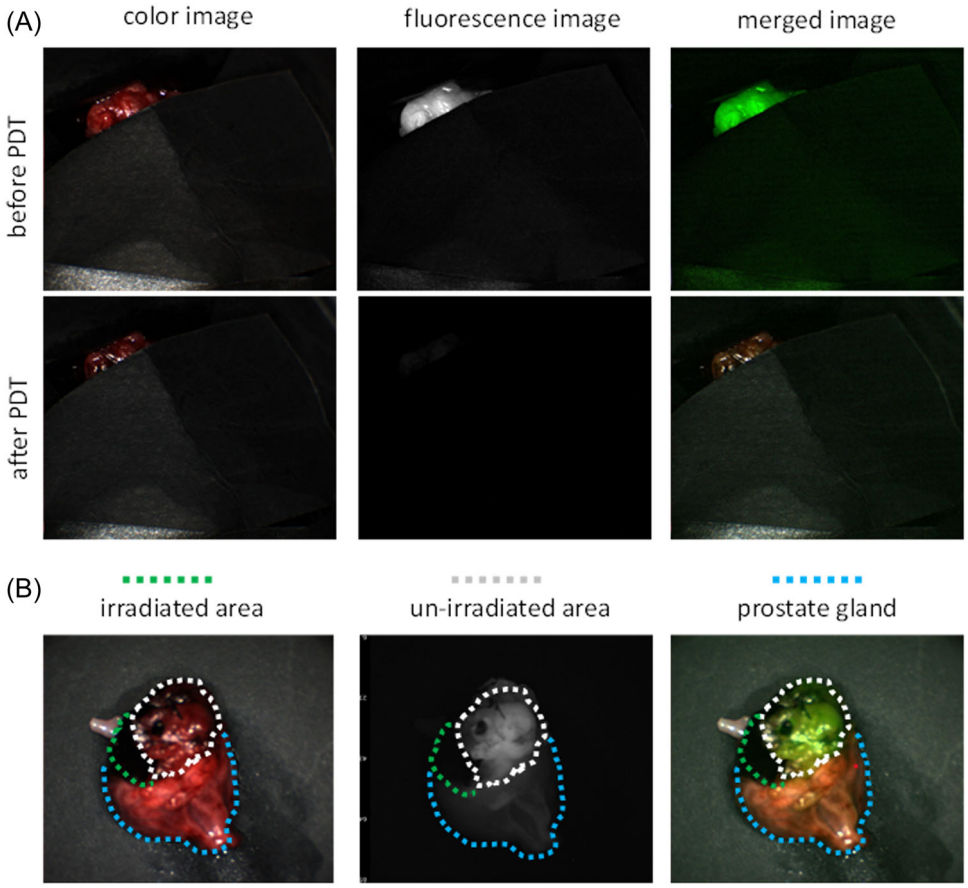

FIGURE 3 Representative FL images of PDT treatment for prostate tumor (dog no. 3). (A) In vivo FL image of prostate tumor before PDT and after PDT treatment, with most of the tumor and majority of the prostate gland covered. (B) Ex vivo FL image of whole prostate after PDT (all cover removed; White circles indicates nonirradiated tumor area, green circles indicates irradiated area and blue circles indicates normal prostate gland.). FL, fluorescence; PDT, photodynamic therapy.

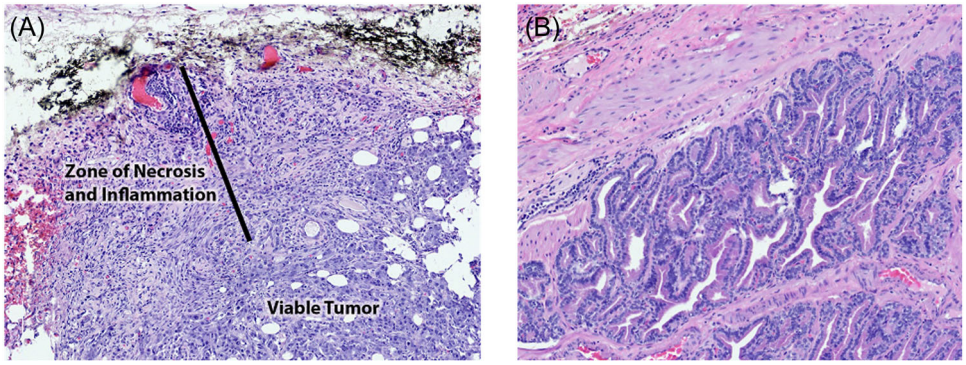

FIGURE 4 Representative H&E images of prostate and prostate tumor from dog no.3. (A) Prostate tumor after PDT treatment. The black dye is a surface dye used to localize the region of PDT laser treatment. The tumor near the surface had necrosis, hemorrhage, and secondary inflammation. The deeper tumor was viable. (B) Normal adjacent prostate with benign prostatic hyperplasia and PDT therapy. There was no evidence of necrosis as a result of the PDT therapy. H&E, hematoxylin and eosin; PDT, photodynamic therapy.

been transfected into prostate cancer cell lines to mimic the high expression of PSMA in human prostate cancer.[48,49] In our earlier studies, we have utilized human prostate cancer cell lines, such as retrovirally transformed PSMA-positive PC3pip cells, LNCaP, and C4-2 cells, and developed heterotopic and orthotopic prostate tumor models in mice for the assessment of PSMA-targeted imaging and therapeutic probes.[27,50] Promising results were observed in the mouse tumor models, but none of these models can fully recapitulate

the features of prostate cancer as it occurs in men. Therefore, we used the dog prostate cancer model[23] to investigate the performance of one of our PSMA-targeted PDT nano agents, AuNPs-Pc158. Our data showed that PSMA expression in dog prostate cancer Ace-1 cells is negligible and we, therefore, transfected Ace-1 cells with human PSMA and obtained Ace-1-hPSMA cells (Supporting Information: Figure S3). Each Ace-1-hPSMA cell had 46,750 PSMA receptors/cell (Figure 1, Table 1). Our previous study has reported that the amount of PSMA receptors in human prostate cancer cells ranged from 13,250/cell (CWR22rv1) to 159,500/cell (MDA PCa2b),[35] therefore, the expression of PSMA receptors by Ace-1-hPSMA is within the range of PSMA expression occurring on human prostate cancer cells derived from spontaneously occurring human prostate cancers. Therefore, Ace-1-hPSMA cells are suitable to establish the canine model for evaluating the efficacy of PSMA-targeted AuNPs-Pc158.

The photosensitizer, Pc158, was covalently conjugated to the surface of 5 nm gold nanoparticles via a cathepsin-cleavable linker that was readily released for FL imaging and PDT upon uptake and cleavage in prostate cancer cells containing cathepsins.[32] Based on the FL imaging results, the PSMA-targeted nano agents can recognize PSMA-expressing prostate cancer and be activated to release fluorescent Pc158, which is completely quenched before being cleaved from the nanoparticles.[32] Compared to the white light images, the fluorescent images revealed a superior contrast between tumor and the normal tissue. The ability to differentiate prostate cancer and normal gland tissue by the PSMA-targeting nano agents enables precise localization of cancer for image-guided partial prostatectomy. The nano agents extravasate from the vasculature into the extracellular tumor microenvironment. The nano agents can then be taken up by Ace-1-hPSMA tumor cells by PSMA receptor-mediated endocytosis. After uptake, the gold nanoparticle-quenched Pc158 would be cleaved by cathepsin in the cancer cells, released, and available for FL. This process was thoroughly investigated in vitro and in vivo with a mouse prostate cancer model and nano agents showed outstanding ability to differentiate PSMA-positive tumors from PSMA-negative tumor and normal tissues.[32]

Notably, in the dog model, in addition to the tumors which had a bright FL signal, fat tissues also had significant fluorescent signal (data not shown), and we confirmed the presence of free Pc158 in the fat tissue by measuring the FL spectrum of fat extractions (Supporting Information: Figure S10). The nonspecific accumulation of Pc158 in the fat tissue may due to the activation of nano agents during circulation in the blood, release of Pc158, and fat accumulation. Further, some of the Pc158 FL distribution in the tissue did not overlap with the nano agent's distribution (Supporting Information: Figure S6). Previous studies have shown that the hydrophobic silicon phthalocyanine has high affinity for the lipid environment.[51] In our nude mouse prostate cancer model, some nonspecific FL signal was detected from the neck area where there is an accumulation of fat in the mice.[32]

Although the injection dose and timing for imaging of nano agents were based on the results from the mouse model, dogs are genetically more heterogenous than most mouse models, differ physiologically from mice, and the optimal conditions for mice may not be the same for the dogs. We were unable to optimize the injection dose and treatment time for PDT outcomes with the limited dog numbers used in this study. Nevertheless, the ability to clearly differentiate tumor tissue from surrounding normal prostate tissue, both inside and outside of the prostate gland, with the nano agents using nonoptimized parameters promises to greatly improve the precision of tumor resection.

NIR light has limited penetration through tissues,[52] and PDT irradiation of tumors showed a necrosis depth of 1–2 mms from the surface. The surrounding tissues that did not take up the nano agents, for example, had no FL signal, were undamaged. The results indicated that PDT with the help of nano agents was effective for focal therapy. Moreover, the photosensitizer was easily detected by the hand-held surgical NIR camera system and could easily be used for FL-guided tumor resection. Image-guided surgery combined with PDT to completely ablate the remaining tumor margins, could dramatically improve the cure rate (as shown in mouse models[16]). Further, it has been demonstrated that activation of photosensitizers can also be achieved by X-rays to overcome the limited penetration of light.[53] Finally, gold nanoparticles are potent radiosensitizers[29] and this approach could allow for rapid identification and maximal resection of tumor tissues followed by more effective radiotherapy due to remaining cancer tissue (or microscopic disease) having taken up the nanoparticles as seen in Supporting Information: Figure S6.

Large animal models with more physiological and anatomic similarities to humans allows us to better assess the performance of nano agents, in both orthotopic tumor FL imaging-guided resection and PDT treatment. The canine model is relatively costly, labor intensive, and less readily available (3–5 year dogs are required); however, the advantages of the dog model outweigh the disadvantages, especially in translational prostate cancer research.[23] For instance, in the assessment of radiosensitizers for imaging-guided radiotherapy, a prostate gland should be large enough for the CT or MR to locate and define the tumor region for precise radiation dose calculation.[54] Furthermore, the orthotopic canine prostate cancer model is excellent for investigating imaging or therapeutic agents for late stage, androgen-independent prostate cancer and metastasis to bone, lymph nodes, and lung.[23]

5 | CONCLUSION

In summary, we have successfully established an orthotropic canine prostate cancer model expressing human PSMA. The tumors grew routinely in immunosuppressed dogs. The prostate cancer cell line, Ace-1, was engineered to express human PSMA, so that the tumors could be recognized by the PSMA-targeted ligands or nano agents. By employing a previously used PSMA-targeted PDT nano agent (AuNPs-Pc158), we demonstrated the ability to differentiate the tumor and normal prostate gland with an FL imaging camera. The cancer-associated protease release of Pc158 enabled spatiotemporal

precise PDT by applying light irradiation to the areas of interest. Histological analysis revealed the presence of tumor in the prostate gland and focal damage induced by PDT and did not produce collateral damage to normal surrounding tissues without uptake of the nanoparticles. The successful use of the PSMA-targeted nano agents for PDT in the dog prostate cancer model holds the potential to advance future investigations of similar agents for image-guided prostatectomy and therapy to support clinical translation.

ACKNOWLEDGMENTS

This research was supported by the National Institute of Health Grant (RO1 EB020353) and the National Foundation of Cancer Research.

CONFLICT OF INTEREST STATEMENT

The authors declare no conflict of interest.

DATA AVAILABILITY STATEMENT

The data that support the findings of this study are available from the corresponding author upon reasonable request.

ORCID

Xinning Wang http://orcid.org/0000-0001-7729-0534
Michael F. Tweedle http://orcid.org/0000-0001-7319-2400
James P. Basilion http://orcid.org/0000-0002-8659-3307

REFERENCES

1. Siegel RL, Miller KD, Fuchs HE, Jemal A. Cancer statistics, 2022. *CA Cancer J Clin*. 2022;72(1):7-33.
2. Kamran SC, Zietman AL. Radiation treatment in prostate cancer: covering the waterfront. *BJU Int*. 2021;128(4):398-407.
3. Terlizzi M, Limkin EJ, Moukasse Y, Blanchard P. Adjuvant or salvage radiation therapy for prostate cancer after prostatectomy: current status, controversies and perspectives. *Cancers*. 2022;14(7):1688.
4. Luo D, Wang X, Zeng S, Ramamurthy G, Burda C, Basilion JP. Prostate-specific membrane antigen targeted gold nanoparticles for prostate cancer radiotherapy: does size matter for targeted particles? *Chem Sci*. 2019;10:8119-8128.
5. Wang X, Huang SS, Heston WDW, Guo H, Wang BC, Basilion JP. Development of targeted near-infrared imaging agents for prostate cancer. *Mol Cancer Ther*. 2014;13(11):2595-2606.
6. Chen X, Li Q, Liu X, et al. Defining a population of stem-like human prostate cancer cells that can generate and propagate castration-resistant prostate cancer. *Clin Cancer Res*. 2016;22(17):4505-4516.
7. Roviello G, Sigala S, Sandhu S, et al. Role of the novel generation of androgen receptor pathway targeted agents in the management of castration-resistant prostate cancer: a literature based meta-analysis of randomized trials. *Eur J Cancer*. 2016;61:111-121.
8. Zhang J, Rakhimbekova A, Duan X, et al. A prostate-specific membrane antigen activated molecular rotor for real-time fluorescence imaging. *Nat Commun*. 2021;12(1):5460.
9. Derks YHW, Löwik DWPM, Sedelaar JPM, et al. PSMA-targeting agents for radio- and fluorescence-guided prostate cancer surgery. *Theranostics*. 2019;9(23):6824-6839.
10. Luo D, Wang X, Walker E, et al. Targeted chemoradiotherapy of prostate cancer using gold nanoclusters with protease activatable monomethyl auristatin E. *ACS Appl Mater Interfaces*. 2022;14(13):14916-14927.
11. Xia L, Meng X, Wen L, et al. A highly specific multiple enhancement theranostic nanoprobe for PET/MRI/PAI image-guided radioisotope combined photothermal therapy in prostate cancer. *Small*. 2021;17:e2100378.
12. Luo D, Johnson A, Wang X, et al. Targeted radiosensitizers for MR-guided radiation therapy of prostate cancer. *Nano Lett*. 2020;20(10):7159-7167.
13. Webster A, Appelt AL, Eminowicz G. Image-guided radiotherapy for pelvic cancers: a review of current evidence and clinical utilisation. *Clin Oncol*. 2020;32(12):805-816.
14. Gong L, Zhang Y, Liu C, Zhang M, Han S. Application of radiosensitizers in cancer radiotherapy. *Int J Nanomedicine*. 2021;16:1083-1102.
15. Xie J, Gong L, Zhu S, Yong Y, Gu Z, Zhao Y. Emerging strategies of Nanomaterial-Mediated tumor radiosensitization. *Adv Mater*. 2019;31(3):e1802244.
16. Wang X, Ramamurthy G, Shirke AA, et al. Photodynamic therapy is an effective adjuvant therapy for image-guided surgery in prostate cancer. *Cancer Res*. 2020;80(2):156-162.
17. Kularatne SA, Thomas M, Myers CH, et al. Evaluation of novel prostate-specific membrane antigen-targeted near-infrared imaging agent for fluorescence-guided surgery of prostate cancer. *Clin Cancer Res*. 2019;25(1):177-187.
18. Mieog JSD, Achterberg FB, Zlitni A, et al. Fundamentals and developments in fluorescence-guided cancer surgery. *Nat Rev Clin Oncol*. 2022;19(1):9-22.
19. Wang F. Modeling human prostate cancer in genetically engineered mice. *Prog Mol Biol Transl Sci*. 2011;100:1-49.
20. Sun F, Báez-Díaz C, Sánchez-Margallo FM. Canine prostate models in preclinical studies of minimally invasive interventions: part I, canine prostate anatomy and prostate cancer models. *Transl Androl Urol*. 2017;6(3):538-546.
21. Tweedle MF, Ding H, Drost WT, et al. Development of an orthotopic canine prostate cancer model expressing human GRPr. *Prostate*. 2018;78:1111-1121.
22. Simmons J, Elshafae S, Keller E, McCauley L, Rosol T. Review of animal models of prostate cancer bone metastasis. *Vet Sci*. 2014;1:16-39.
23. Keller JM, Schade GR, Ives K, et al. A novel canine model for prostate cancer. *Prostate*. 2013;73(9):952-959.
24. Wang Y, Abenojar EC, Wang J, et al. Development of a novel castration-resistant orthotopic prostate cancer model in New Zealand White rabbit. *Prostate*. 2022;82(6):695-705.
25. Rosol TJ, Tannehill-Gregg SH, LeRoy BE, Mandl S, Contag CH. Animal models of bone metastasis. *Cancer*. 2003;97(3 suppl):748-757.
26. Liu G, Banerjee SR, Yang X, et al. A dextran-based probe for the targeted magnetic resonance imaging of tumours expressing prostate-specific membrane antigen. *Nat Biomed Eng*. 2017;1:977-982.
27. Wang X, Shirke A, Walker E, et al. Small molecule-based prodrug targeting prostate specific membrane antigen for the treatment of prostate cancer. *Cancers*. 2021;13(3):417.
28. Wang X, Tsui B, Ramamurthy G, et al. Theranostic agents for photodynamic therapy of prostate cancer by targeting prostate-specific membrane antigen. *Mol Cancer Ther*. 2016;15(8):1834-1844.
29. Luo D, Wang X, Zeng S, Ramamurthy G, Burda C, Basilion JP. Targeted gold nanocluster-enhanced radiotherapy of prostate cancer. *Small*. 2019;15(34):1900968.
30. Li H, Luo D, Yuan C, et al. Magnetic resonance imaging of PSMA-positive prostate cancer by a targeted and activatable Gd(III) MR contrast agent. *J Am Chem Soc*. 2021;143(41):17097-17108.
31. Mangadlao JD, Wang X, McCleese C, et al. Prostate-specific membrane antigen targeted gold nanoparticles for theranostics of prostate cancer. *ACS Nano*. 2018;12(4):3714-3725.

32. Luo D, Wang X, Walker E, et al. Nanoparticles yield increased drug uptake and therapeutic efficacy upon sequential near-infrared irradiation. *ACS Nano*. 2020;14(11):15193-15203.
33. LeRoy BE, Thudi NK, Nadella MVP, et al. New bone formation and osteolysis by a metastatic, highly invasive canine prostate carcinoma xenograft. *Prostate*. 2006;66:1213-1222.
34. Wu LY, Johnson JM, Simmons JK, et al. Biochemical characterization of prostate-specific membrane antigen from canine prostate carcinoma cells. *Prostate*. 2014;74(5):451-457.
35. Wang X, Ma D, Olson WC, Heston WDW. In vitro and in vivo responses of advanced prostate tumors to PSMA ADC, an auristatin-conjugated antibody to prostate-specific membrane antigen. *Mol Cancer Ther*. 2011;10(9):1728-1739.
36. Kozikowski AP, Nan F, Conti P, et al. Design of remarkably simple, yet potent urea-based inhibitors of glutamate carboxypeptidase II (NAALADase). *J Med Chem*. 2001;44(3):298-301.
37. Sharma V, McNeill JH. To scale or not to scale: the principles of dose extrapolation. *Br J Pharmacol*. 2009;157(6):907-921.
38. Perera RH, de Leon A, Wang X, et al. Real time ultrasound molecular imaging of prostate cancer with PSMA-targeted nanobubbles. *Nanomedicine*. 2020;28:102213.
39. Davis MI, Bennett MJ, Thomas LM, Bjorkman PJ. Crystal structure of prostate-specific membrane antigen, a tumor marker and peptidase. *Proc Natl Acad Sci USA*. 2005;102(17):5981-5986.
40. Schülke N, Varlamova OA, Donovan GP, et al. The homodimer of prostate-specific membrane antigen is a functional target for cancer therapy. *Proc Natl Acad Sci USA*. 2003;100(22):12590-12595.
41. Mitsunaga M, Ogawa M, Kosaka N, Rosenblum LT, Choyke PL, Kobayashi H. Cancer cell-selective in vivo near infrared photoimmunotherapy targeting specific membrane molecules. *Nature Med*. 2011;17(12):1685-1691.
42. Henderson BW, Gollnick SO, Snyder JW, et al. Choice of oxygen-conserving treatment regimen determines the inflammatory response and outcome of photodynamic therapy of tumors. *Cancer Res*. 2004;64(6):2120-2126.
43. Colussi VC, Feyes DK, Mulvihill JW, et al. Phthalocyanine 4 (Pc 4) photodynamic therapy of human OVCAR-3 tumor xenografts. *Photochem Photobiol*. 1999;69(2):236-241.
44. Whitacre CM, Feyes DK, Satoh T, et al. Photodynamic therapy with the phthalocyanine photosensitizer Pc 4 of SW480 human colon cancer xenografts in athymic mice. *Clin Cancer Res*. 2000;6(5):2021-2027.
45. Tazawa H, Shigeyasu K, Noma K, et al. Tumor-targeted fluorescence labeling systems for cancer diagnosis and treatment. *Cancer Sci*. 2022;113(6):1919-1929.
46. Ngen EJ, Chen Y, Azad BB, et al. Prostate-specific membrane antigen (PSMA)-targeted photodynamic therapy enhances the delivery of PSMA-targeted magnetic nanoparticles to PSMA-expressing prostate tumors. *Nanotheranostics*. 2021;5(2):182-196.
47. Nguyen L, Li M, Woo S, You Y. Development of prodrugs for PDT-based combination therapy using a singlet-oxygen-sensitive linker and quantitative systems pharmacology. *J Clin Med*. 2019;8(12):2198.
48. Nascimento-Gonçalves E, Faustino-Rocha AI, Seixas F, et al. Modelling human prostate cancer: rat models. *Life Sci*. 2018;203:210-224.
49. Risbridger GP, Toivanen R, Taylor RA. Preclinical models of prostate cancer: patient-derived xenografts, organoids, and other explant models. *Cold Spring Harbor Perspect Med*. 2018;8(8):a030536.
50. Wang X, Sun R, Wang J, et al. A low molecular weight multifunctional theranostic molecule for the treatment of prostate cancer. *Theranostics*. 2022;12(5):2335-2350.
51. Cheng Y, Meyers JD, Broome AM, Kenney ME, Basilion JP, Burda C. Deep penetration of a PDT drug into tumors by noncovalent drug-gold nanoparticle conjugates. *J Am Chem Soc*. 2011;133(8):2583-2591.
52. Maruoka Y, Nagaya T, Sato K, et al. Near infrared photoimmunotherapy with combined exposure of external and interstitial light sources. *Mol Pharm*. 2018;15(9):3634-3641.
53. Yu X, Liu X, Wu W, et al. CT/MRI-guided synergistic radiotherapy and x-ray inducible photodynamic therapy using Tb-doped Gd-W-nanoscintillators. *Angew Chem Int Ed*. 2019;58(7):2017-2022.
54. Zhou Z, Deng H, Yang W, et al. Early stratification of radiotherapy response by activatable inflammation magnetic resonance imaging. *Nat Commun*. 2020;11(1):3032.

SUPPORTING INFORMATION

Additional supporting information can be found online in the Supporting Information section at the end of this article.

How to cite this article: Luo D, Wang X, Ramamurthy G, et al. Evaluation of a photodynamic therapy agent using a canine prostate cancer model. *The Prostate*. 2023;83:1176-1185. doi:10.1002/pros.24560